Title

Fabrication of Core—Shell Nanotube Array for Artificial Photosynthesis Featuring an Ultrathin Composite Separation Membrane

Journal

ACS Nano, 12(1)

ISSN

1936-0851

Authors

Edri, Eran

Aloni, Shaul

Frei, Heinz

Publication Date

2018-01-23

DOI

10.1021/acsnano.7b07125

Peer reviewed

Fabrication of Core-Shell Nanotube Array for Artificial Photosynthesis Featuring Ultrathin Composite Separation Membrane

Eran Edri[a], Shaul Aloni[b] and Heinz Frei[a*]

[a] Molecular Biophysics and Integrated Bioimaging Division and [b] Molecular Foundry Division, Lawrence Berkeley National Laboratory, University of California, Berkeley, CA 94720

HMFrei@lbl.gov

(*ACS Nano*, accepted)

Abstract

Macroscale arrays of cobalt oxide-silica core-shell nanotubes with high aspect ratio and ultrathin walls of less than 20 nm have been fabricated. The silica shells feature embedded *oligo*-para(phenylene vinylene) molecules for charge transport across the insulating silica layer, which is tightly controlled by their electronic properties. The assembly is based on the use of sacrificial Si nanorod array template combined with atomic layer deposition, covalent anchoring of organic wire molecules, and dry cryo-etching. High resolution TEM imaging of samples prepared by microtome affords structural details of single core-shell nanotubes. The integrity of silica-embedded organic wire molecules exposed to atomic layer deposition, thermal treatment, and harsh etching procedures is demonstrated by grazing angle ATR FT-IR, FT-Raman, and XPS spectroscopy. The inorganic oxide-based core-shell nanotubes with ultrathin gas impermeable, proton conducting silica shells functionalized by molecular wires open up complete nanoscale photosynthetic units for CO_2 reduction by H_2O under membrane separation. Arrays of massive numbers of such core-shell nanotube units afford a design that extends the separation of the incompatible H_2O oxidation and CO_2 reduction catalysis environments across the continuum of length scales from nanometers to centimeters.

Keywords: Artificial photosynthesis, nanotube array, core-shell, ultrathin silica membrane, molecular wires

Scalability of artificial photosystems at the unprecedented level of several terawatts, which is imperative for impact on global fuel consumption, requires keeping balance-of-systems components at a minimum while enabling manufacturing on a massive scale. Natural photosynthesis embodies these requirements as the only existing technology for producing energy-dense chemicals on the terawatt scale. Plant and bacterial photosystems have as key design feature the closing of the cycle of water oxidation and formation of primary reduction intermediates on the shortest possible length scale, the nanometer scale, while separating the incompatible redox environments by an ultrathin membrane.[1,2] This design aspect of natural photosynthesis inspires a synthetic nanoscale system for completing the cycle of light-driven CO_2 reduction by H_2O under membrane separation that would avoid energy losses caused by ion transport resistance associated with macroscale redox cycles, and minimize efficiency-degrading back reactions and charge transport losses, each likely to prove essential for enabling the required scalability.

For visible light driven overall water splitting, first complete, bias-free integrated artificial photosystems reported recently include visible light water splitting at triple junction amorphous silicon (a-Si),[3] tandem cells made of III-V semiconducting materials,[4-7] tandem cells consisting of WO_3 or Fe_2O_3/dye,[8] $BiVO_4$/a-Si [9] or Fe_2O_3/a-Si,[10] and 2-photon TiO_2/Si nanowire or n-WO_3/np$^+$Si microwire arrays.[11-13] These systems close the photosynthetic water splitting cycle on the macroscale, some at high power efficiencies between 5 and 15% for extended periods of time, and all featuring Earth abundant components.[3-5,7,9,14,15] Among them, one possesses a membrane for separating the evolving hydrogen from oxygen.[4,5,16] Despite the very substantial advances, based on criteria for minimal balance of systems and manufacturability, none of these designs are suitable for scale-up to the unprecedented level of several terawatts, which is necessary for impact on fuel consumption. With regard to solar light-driven reduction of CO_2 by H_2O, photovoltaic-assisted systems with high power

efficiency of up to 10% have been reported,[17-19] one operating under membrane separation of products.[19] While the high efficiency for carbon monoxide or formic acid generation establishes an important milestone for CO_2 to fuel conversion, these systems are not scalable at the required level because they use noble metal electrocatalysts and a balance-of-systems-intensive PV-assisted electrosynthetic cell approach.

We are developing nanoscale photosynthetic assemblies for coupling the catalysis for CO_2 reduction with the H_2O oxidation half reaction, taking an inorganic molecular approach that utilizes heterobinuclear units such as $ZrOCo^{II}$ as light absorber coupled to metal oxide cluster catalysts.[20,21] For one such system in which the $ZrOCo^{II}$ unit is coupled to an Ir oxide nanocluster on silica nanopore surface, photoexcitation in the presence of a carbon dioxide–water gas mixture affords the conversion of CO_2 to CO under oxidation of H_2O to O_2, albeit without membrane separation.[22] To accomplish the photocatalytic cycle of CO_2 reduction by H_2O under membrane separation using this inorganic oxide materials approach, we propose a Co oxide – silica core-shell nanotube geometry as sketched in Figure 1. The inside surface of the Co oxide nanotube core would provide the catalytic sites for H_2O oxidation, which are separated from light absorber and sites of CO_2 reduction on the outside by an ultrathin dense phase silica layer. The latter acts as proton conducting, O_2 impermeable membrane as demonstrated in previous work.[23] Tight, molecular-level control of charge transfer between light absorber and Co oxide nanotube catalyst is accomplished by *oligo*-para(phenylene vinylene) molecules with 3 aryl units embedded in the silica shell (abbrev. PV3, 2 nm length, Figure 1).[24-27] This approach addresses the requirements of robustness and tunability of the electronic properties of the photosystem components with the objective of converting the maximum fraction of the solar photon energy into chemical energy of the fuel. While, as such, the synthetic method allows for a broad choice of core-shell morphology, we are using nanotube geometry because it offers the opportunity of assembling macroscale arrays

of enormous numbers of nanotubes, each operating as independent photosynthetic unit while at the same time providing separation of evolving O_2 and reduced CO_2 products on all length scales from nano to centimeters (Figure 1).

Existing approaches for making a tube array include direct solvothermal treatment,[28,29] vapor phase deposition,[30] a deposition-conversion method,[31,32] or a combination of hydrothermal and vapor phase deposition methods.[33] Alternatively, templates such as rods, or anodized alumina are coated with the chosen material, and the support etched away.[34-36] These methods provide tubes of several micron length with walls as thin as eight nm and a diameter of ten to hundreds of nm. However, a material-flexible and scalable method for fabricating free-standing core-shell tube array with fine control of characteristic length scales has remained a challenge. Microsphere lithography is a viable route for fabricating an array of aligned Si rods with high aspect ratio.[37] A method for reducing surface roughness and controlling the morphology is provided by combining dry etching and etching-gases of specific compositions.[38,39] The power of atomic layer deposition (ALD) to conformally coat high aspect ratio structures has been demonstrated.[40] At the same time the number of materials that can be deposited by ALD is continuously growing.[41,42]

In this paper, we report the fabrication of macroscale arrays of free-standing high aspect ratio Co oxide – silica core-shell nanotubes featuring unprecedented ultrathin walls (< 20 nm) with embedded charge conducting PV3 wire molecules. The structural integrity of the silica-embedded wire molecules exposed to ALD, thermal treatment and dry cryo-etching procedures upon assembly of the array is demonstrated by grazing angle ATR FT-IR, FT-Raman, and XPS spectroscopy. Structural details of single core-shell nanotubes are revealed by high resolution TEM imaging of slices obtained by microtome. Combined with all-inorganic light absorbers, methods of coupling to metal oxide catalysts for H_2O oxidation and CO_2 reduction, and detailed knowledge of the charge transfer properties of silica-embedded

molecular wire developed in previous effort,[20-27] the core-shell nanotube arrays can be functionalized to give complete artificial photosystems that will allow closing of the photosynthetic cycle of CO_2 reduction by H_2O on the nanoscale under membrane separation that extends to the macroscale. The approach potentially affords toleration of structural defects thereby relaxing fabrication method requirements.

Core-shell nanotube array synthesis

Nanotube arrays were formed by combination of microsphere lithography, dry cryo-etching, room temperature etching, and ALD. Polystyrene based beads of 1 μm diameter were spin-coated on plasma or piranha cleaned Si wafer from ethanol solution and formed a uniform single layer of beads (>85% of the area is a single layer based on optical microscope imaging). The beads are densely packed and form tens of micron-sized crystalline arrays as can be seen in Figure 2A. The beads are shrunk to approximately half their diameter by plasma etching in O_2 (Figure 2A lower inset; etching can be stopped at earlier stage to form larger beads but etching of more than 50% usually leads to deformation of the beads). The bead-coated Si wafer is than cooled down to -125°C and a plasma mixture of SF_6 and O_2 is used to dry etch the Si to form an array of 3-5 μm long microrods (length controlled by etching time). The beads are removed from the top with O_2 plasma (Figure 2C) and the rods coated with Co_3O_4, SiO_2 and Al_2O_3, by ALD. For samples containing PV3 wire molecules embedded in the ultrathin silica shell, the molecules are covalently anchored on the Co_3O_4 tube surface prior to SiO_2 casting using the peptide coupling agent HCTU (O-(6-chlorobenzotriazol-1-yl)-,N,N,N,N-tatramethyluronium hexafluorophosphate), as described previously.[25] Vertical orientation of the PV3 molecules on the Co_3O_4 tube surface is imposed by use of a the tripodal anchor tris(hydroxymethyl) aminomethane (abbrev. tripod) and of a sulfonate substituent on the opposite end of the wire molecule that is electrostatically repelled from the negatively charge

Co oxide surface (abbrev. PV3_tripod for wire molecule with attached anchor).[26] Subsequently, the Co oxide-silica covered Si rods are selectively etched at the top using high pressure SF_6 / CHF_3 plasma etching to form open-ended rods (Figure 2D). Alternatively, the removable polymer PMMA (poly(methyl methacrylate)) is spin-coated, the top of the rods exposed and opened using a similar etching procedure (Figure S1). The inner Si core is cryo-etched with SF_6. Partially etched rod-tubes are shown in Figure 2E, fully etched tubes in Figure 2F and 2G. Ten minute rinse in acetone will remove the PMMA polymer completely.

Structural characterization of core-shell nanotube array

Grazing angle attenuated total reflection (GAATR) FT-IR spectra shown in Figure 3A confirm the attachment of PV3_tripod to the Co_3O_4 tube surface and the integrity of the molecular structure after SiO_2 deposition by plasma assisted ALD. While the spectra of Co_3O_4 on Si rod array (abbrev. Si/Co_3O_4), trace (a), and pure SiO_2 coated on Si/Co_3O_4 rods (trace (b)) do not show any distinct infrared bands in the 950-1250 cm^{-1} region, spectra recorded after anchoring of PV3_tripod exhibit characteristic molecular absorptions. Specifically, bands at 961 and 970 cm^{-1} shown in trace (c) are assigned to =C-H stretching vibrations of the vinyl linkages. The 1009 cm^{-1} band is the para-di-substituted phenyl group C-H in-plane bending mode, and the 1036 cm^{-1} peak is assigned to C-S aryl stretching mode. These bands, which remain intact after casting of silica (trace (d)), closely match the absorbance spectrum of neat PV3_tripod dispersed in KBr, as shown in trace (e).

X-ray photoelectron spectroscopy in the S 2p region of PV3_tripod on Si/Co_3O_4 rods shows a peak at 169.8 eV (Figure 3B trace (b)), which is absent before PV3_tripod attachment (trace (a)). A similar peak is found after SiO_2 deposition, i.e. for samples with SiO_2-encapsulated PV3_tripod on Si/Co_3O_4 (trace (d)) albeit shifted to higher binding energies (171.3 eV) due to the insulating silica environment. The absence of this peak for SiO_2 coated

Co_3O_4 without attached PV3_tripod (trace (c)) confirms the assignment. Observations in the N 1s region support the conclusion that the PV3_tripod molecules are attached to Co_3O_4. Namely, Figure 3C trace (b) shows the N 1s peak at 401.5 eV, which we assign to amide (the shoulder at 403.9 eV is most likely ammonium attributed to some residual HCTU coupling agent). After deposition of SiO_2 onto Si rod/Co_3O_4 array without anchored PV3 wire molecules, nitrogen is found from the silica ALD process with two distinctive peaks as shown in Figure 3C trace (c). These signals are attributed to N from residual Si amido precursor. For spectra recorded after depositing the silica layer onto arrays with PV3 wires attached, this N signal from the precursor is overwhelmed by the amide N of the linked wire molecule at 401.5 eV (trace (d)). We conclude from the FT-IR and XPS results that PV3_tripod molecules are attached and encapsulated in the SiO_2 layer of the core-shell nanotubes, in agreement with the findings for corresponding planar constructs.[25]

For nanoscale resolution imaging, the nanotubes were transferred to a holey carbon TEM grid by brushing a tube onto a grid, with the resulting image shown in Figure 4A. While this confirms that the inner volume of the tube is empty, it does not allow measurement and evaluation of the composition of the tube wall. To investigate the nanometer scale structure, the tube array is encapsulated in a uniform, flexible organic layer by room temperature vapor phase deposition of parylene-C. Depositing 4-5 μm of the polymer allows removal of the layer from the Si wafer by peel-off. The lamella containing the tubes is sliced by microtome to 25-100 nm thick slices in transverse and longitudinal direction (with respect to the tube long axis) that can be studied in the TEM. Figure 4B shows a low magnification HAADF-STEM image of a transverse cross-section of part of a tube array, with a high magnification HAADF-STEM image of a single tube presented in Figure 4D. Both images confirm that the Si core was removed by etching. A longitudinal slice STEM image of three tubes is shown in Figure 4C. The walls of the tubes are broken to ~100 nm fragments from the sample preparation

processing. However, the general structure is preserved by embodiment in parylene-C, which allows us to study the tube walls along the long axis. An EDX map shows a higher concentration of Co near the top of the tube than at the bottom, possibly as a result of the Si core etching step also resulting in some etching of the Co_3O_4 layer. At the same time, the SiO_2 layer appears to be uniform throughout the tube layer, affirming the protecting role of the Al_2O_3 layer. High resolution TEM image (Figure 4E) shows the crystalline 12 nm thick Co_3O_4 layer on the inner side of the tube, coated with a 2 nm thick SiO_2 layer and protected by a 10 nm thick Al_2O_3 layer on the outer side of the tube. The crystallinity of the Co_3O_4 is evident in the circular diffraction pattern shown in the inset of Figure 4B, and by FFT taken from the inner volume wall of the tube (inset of Figure 4E). A high magnification HAADF-STEM image of a transverse cross section of a tube wall is presented in Figure 4F. The three layers making the tube walls are distinguishable by their different contrast, with a total thickness of 20 nm. The granular nature of the inner Co_3O_4 tube wall is evident from the image.

Following complete etching of the Si rods, the core-shell nanotubes were mechanically scraped off the Si support and the FT-Raman spectra of the resulting powder recorded. As can be seen from Figure 5 trace (a), the spectrum of the PV3_tripod molecules embedded in the 2 nm silica shell agrees well with that of the free molecules in powder form (trace (b)). The amide I band at 1630 cm^{-1}, characteristic aromatic ring breathing modes at 1590 and 1553 cm^{-1} as well as the sulfonic group stretching modes at 1323, 1192 and 1175 cm^{-1} are seen.[43] We conclude that the organic wire molecules cast into ultrathin dense phase silica retain their structural integrity during the etching process.

Towards a fully functional nanotube array

In previous work, we have developed all-inorganic light absorbers coupled to metal oxide nanoparticle catalysts and evaluated charge transport properties of silica membrane-

embedded molecular wires designed for incorporation into the Co oxide-silica core-shell nanotube assembly reported here for obtaining a complete artificial photosynthetic system. Specifically, Co_3O_4 nanotubes were shown to serve as efficient water oxidation catalysts under visible light sensitization (turnover frequency 0.02 O_2 s^{-1} surface Co site).[23] Heterobinuclear metal-to-metal charge-transfer (MMCT) units anchored on concave or convex silica nanoparticle surfaces were shown to act as light absorbers for driving metal oxide nanoparticle catalysts for H_2O oxidation [22,44] or CO_2 reduction.[45] Coupling of the nanoparticle catalyst to the proper metal center of the heterobinuclear light absorber (Co donor or Zr acceptor center) was enabled by photodeposition engaging the spatial directionality of the visible MMCT transition for assembly of the catalyst cluster. In the case of the $ZrOCo^{II}$ group, the resulting $ZrOCo^{II}$-IrO_x unit affords closing of the photosynthetic cycle of CO_2 reduction by H_2O.[22] Properties of silica embedded wire molecules were determined by transient optical absorption spectroscopy, which revealed ultrafast (255 ps) hole transfer from visible light absorber to Co_3O_4 across a 2 nm silica membrane with embedded PV3_tripod wire molecules.[27] The charge flux through the embedded wires was quantified by visible light photosensitized current measurements in short circuit configuration using planar, cm^2-sized electrodes consisting of SiO_2-encapsulated PV3_tripod on Pt/Co_3O_4.[25] The photosensitization experiments using light absorbers covering a range of redox potentials demonstrated that the orbital energetics of the embedded wire molecules control charge transfer across the silica membrane.[25] The proton transmission was evaluated by cyclic voltammetry of amorphous silica layers prepared on Pt electrodes (using the ALD methods applied for the nanotube fabrication) in aqueous solution, and O_2 impermeability for silica thickness above 2 nm confirmed.[23] With these components established and quantitatively evaluated, the assembly of fully functionalized core-shell nanotube arrays can now be pursued.

Conclusions

A simple and scalable top down fabrication method of an array of free-standing core-shell tubes is presented. While the array is fabricated on cm-scale, individual tube diameter is a few hundreds of nanometers wide, and the tube walls are a few tens of nanometers. By using a Si rod array as template, and a combination of atomic layer deposition and cryo-etching, control of the characteristic length scales of the components spans eight orders of magnitude and allows to address two major scientific challenges of artificial photosystems. One is closing of the photosynthetic cycle on the shorted possible length scale under membrane separation accomplished by the 2 nm-sized proton conducting, gas impermeable silica shells with embedded molecular wires that offer precise control of electron transfer. A second challenge is the extension of the separation of catalytic sites of water oxidation from the sites of CO_2 reduction across the continuum of length scales from nanometers to centimeters and beyond. The Si nanorod array template method applied here accomplishes the goal except that permanent product separation will require addition of top and bottom enclosure with the nanotube openings piercing through them, as sketched in Figure 1. An important advantage of the nanotube array design is the fact that each of the enormous number of core-shell nanotubes operates as an independent photosynthetic unit, providing robustness of the macroscale system through redundancy.

Methods

Synthesis: Cesium 4-((E)-4-((E)-4-((sulfonatostyryl)styryl)benzoate) was synthesized as described previously,[26] and the surface anchoring group (tris(hydroxymethyl) aminomethane (99%, Alfa Aesar A18494, abbrev. tripod) was attached using HCTU coupling agent (O-(6-chlorobenzotriazol-1-yl)-,N,N,N,N-tatramethyluronium hexafluorophosphate; Sigma Aldrich Cat. No. 8510120025) in dimethyl formamide solution (anhydrous 99.8%; Sigma-Aldrich Cat.

No. 227056). The product, abbreviated PV3_tripod, and HCTU were stored in the dark in a N_2 glove box. All chemicals were used without further purification, unless stated otherwise.

Polystyrene based beads were purchased from Sigma-Aldrich (89904-5ML-F), 1 mL of the aqueous suspension was evaporated in an oven at 70°C and ethanol (pure, 200 proof; Sigma-Aldrich Cat. No. 792780) of the same volume was added to the solids. The mixture was sonicated for ~2 hrs until a milky uniform suspension was obtained. Before each use, the suspension was sonicated for at least 20 min.

In a Class 100 cleanroom environment, a 100 mm Si wafer (prime grade; single side polished) was cleaned by either 2 hr of sulfuric acid piranha solution (3:1 by volume sulfuric acid and 30% wt. hydrogen peroxide. CAUTION: the mixing of sulfuric acid and hydrogen peroxide is a very exothermic reaction and leads to release of corrosive fumes. Care should be taken when handling piranha solution), or O_2 plasma cleaning (25°C; 250 W; 100 mTorr; 100 SCCM O_2; 10 min.) and immediately used to spin cast 360 μL of the polystyrene dispersion (Step 1: 300 RPM/sec; 300 RPM; 20 sec. Step 2: 300 RPM/sec; 1200 RPM; 80 sec). The polystyrene beads were shrunk from about 1 μm in diameter to about 0.5-0.6 μm by O_2 plasma (25°C; 100 W; 100 mTorr; 100 SCCM O_2; 3:30 min).

The ICP-RIE (inductively coupled plasma – reactive ion edging) chamber was cooled down to -125°C and the wafer etched with SF_6:O_2 plasma (-125°C; plasma ignited with 50 W forward ICP for 5 sec followed with 15W ICP for 1:50 min with 1000 W RF power; 6 mTorr; 42:8 SF_6:O_2 SCCM) using the beads as mask to form Si rod array. The beads were removed by O_2 plasma cleaning (25°C; 250 W; 100 mTorr; 100 SCCM O_2; 10 min.).

The Si rods are coated with Co_3O_4 by ALD at 40°C (Oxford FlexAl-Plasma Enhanced Atomic Layer Deposition system). Bis(cyclopentadienyl)cobalt(II) was used as Co precursor (cobaltocene, $CoCp_2$; min 98% STREM Chemicals Inc., heated to 80°C and bubbled with 200 SCCM high purity Ar during pulse). A continuous oxygen flow of 60 SCCM was

kept during the deposition process. $CoCp_2$ dose was 5 sec long, followed by 5 sec of purging. Oxygen plasma half-cycle was 1 sec pre-plasma, 5 sec plasma (300 W) and 15 sec purging.

After cutting to 2.5x2.5 cm fragments, a sample is warmed up to 120°C under vacuum in a Schlenk flask and transferred to a N_2 glove box. In another Schlenk reaction flask, PV3_tripod (5.9 mg) and HCTU (18.0 mg) are evacuated and cooled to 0°C. 10 mL of anhydrous DMF is syringed in to form a transparent solution that is stirred to dissolve all solids. The flask is subsequently transferred to a N_2 glove box and the solution added to the reaction flask with the Co_3O_4-coated Si rod sample. 20µL of N-ethyldiisopropylamine is added and the solution stirred for 24 h, after which it is rinsed with excess deionized water and dried by N_2 stream.

SiO_2 layer is deposited around the PV3_tripod molecules by ALD using a procedure reported previously.[25] In short, at 40°C and 5 SCCM flow of ultrapure Ar (chamber pressure of ~80 mTorr), a 0.05 sec pulse of Si precursor (tris-dimethylaminosilane (99+% STREM chemicals; kept at ambient temperature)) was introduced alongside closing the chamber exhaust valve for 40 sec. The chamber was purged with 100 SCCM Ar for 15 sec. Before plasma was started, the chamber was purged with 5 SCCM of oxygen flow (alongside 3 SCCM Ar flow, chamber pressure ~ 200 mTorr) for 20 sec and then plasma (100 W) was ignited and run for 30 sec followed by 35 sec of Ar purging (15 sec at 5 SCCM and 20 sec at 100 SCCM). These steps constitute a single ALD cycle. Normally, 20 cycles are used which result in 2 nm thick SiO_2 layer.

A protective Al_2O_3 layer of 5 nm is subsequently deposited by ALD (20 SCCM; 0.015 sec trimethyl aluminum; purge 30 sec; 0.015 sec H_2O pulse; purge 30 sec; 80°C). When the protective polymer PMMA is used, HMDS is first spin-coated to improve wetting (2000 RPM; 2000 RPM/sec; 2 min), which is immediately followed by spin coating 0.8 mL of PMMA (950 A11; MicroChem; Step 1: 500 RPM/sec; 500 RPM; 10 sec. Step 2: 500 RPM/sec;

2500 RPM; 2 min) and baking for 1 min at 100°C. The top of the rods are then etched by RIE (SF_6: CHF_3 10: 50 SCCM; 75 W; 100 mTorr 2:30 hr) and the core etched with SF_6 (-120°C; plasma ignited with 30 W forward ICP for 5 sec followed with 20W ICP for 1:50 min with 1000 W RF power; 6 mTorr; 48:2 SF_6:O_2 SCCM) to form ~3-5 μm long tubes with 0.5-0.6 diameter and ~20 nm thick walls. The PMMA is removed by immersing the sample in acetone for 15 min and careful drying by N_2 stream.

Alternatively, directed etching at the top of the rods, without PMMA, can be performed by high pressure RIE (SF_6: CHF_3 10: 50 SCCM; 75 W; 100 mTorr; 1 h), followed by ICP-RIE Si core etching. This usually leads to under-etching for rods of several micron length, but can be used for 1-2 μm long rods.

X-ray photoelectron spectroscopy (XPS) was performed with Kratos Axis Ultra DLD system using a monochromatic Al K_α source ($h\nu$ = 1486.6 eV), operated at 225 W at a takeoff angle of 0˚ relative to the surface normal, and pass energy for narrow scan spectra of 20 eV. Spectra analysis was done with CasaXPS V2.3.

Grazing angle attenuated total reflection (GAATR) FT-IR spectra were measured with a Bruker Vertex 70 instrument equipped with liquid nitrogen cooled MCT detector and a Harrick VariGATR™ Grazing Angle Accessory with Ge single reflection ATR crystal. All spectra were recorded at 62.5° incident angle and 4 cm^{-1} resolution. Baseline was measured as ATR crystal/air.

FT-Raman spectroscopy was collected with Bruker IFS66V instrument equipped with FRA-106 Raman accessory. Powder samples of tubes were prepared by scraping the tubes from the Si support surface with a metallic blade. Neat PV3_tripod powder was measured at 4 cm^{-1}

resolution (80 mW 1064 nm Nd:Yag laser radiation) by collecting 1024 scans, while tube-powder was measured at 2 cm^{-1} (152 mW, 25,600 scans).

Transmission electron microscopy. For sample preparation, a tube array supported by a Si wafer was placed in a PDS 2010 evaporation chamber. The tube array is embedded in 4-5 μm parylene-C by evaporation. The parylene is carefully peeled-off the Si wafer, preserving the embedded tubes as indicated by the brownish color of the film and inspection under an optical microscope. A few (between 5 and 9) small (2 x 2 mm) squares are cut from the peeled-off layer and stacked one on top of the other on a smooth Teflon cover. A few drops of UV-curable epoxy are placed on the sample and cured to make a glued stack of parylene films. The stack is put in a small vacuum chamber for rough pumping for a few minutes to remove bubbles as much as possible. After preliminary UV curing, the stack is completely cured in an oven at 60°C for another 24 h. When hardening is complete, the stack is cut from the Teflon cover and inserted into a hole drilled in a pre-made epoxy resin either with transverse plan view orientation or longitudinal cross section orientation (with respect to the parylene lamella and tube long axis). The hole is filed with a drop of UV-curable epoxy mentioned above and the same curing procedure is repeated. Thin slices of the embedded parylene lamella are prepared by a microtome and collected on a 400 mesh Cu TEM grid. Prior to imaging the samples were coated with a thin layer of carbon by evaporation.

TEM and scanning TEM (STEM) imaging is carried out on a JEOL microscope at 200 kV either in high-resolution TEM mode or STEM mode. EDS spectra were collected using a Bruker windowless EDS detector with a solid angle of 0.7 steradians and a double tilt holder.

Scanning electron microscopy was carried with Zeiss ULTRA-55 featuring an InLens detector and using a low acceleration voltage of 2-5 keV in order to minimize charging of the sample. The micro tubes are sensitive to radiation damage and crumble after excessive scanning (usually beam damage is observed after a few minutes of scanning). To reduce damage, the image was focused prior to positioning the beam to scan an area of interest in order to ensure that the images are of a fresh, not previously irradiated micro-tube region.

Acknowledgment

This work was supported by the Director, Office of Science, Office of Basic Energy Sciences, Division of Chemical, Geological and Biosciences of the U.S. Department of Energy under Contract No. DE-AC02-05CH11231. Portions of this work (plasma enhanced atomic layer deposition, micro-sphere lithography, dry etching, scanning and transmission electron microscopy including sample preparation) were performed as a User Project at The Molecular Foundry, Lawrence Berkeley National Laboratory, which is supported by the Office of Science, Office of Basic Energy Sciences. Portion of the work (XPS measurements, GAATR-FT-IR) was performed at the Joint Center for Artificial Photosynthesis, a DOE Energy Innovation Hub, supported through the Office of Science of the U.S. Department of Energy under Award No. DE-SC0004993. The authors thank D. Olynick for guidance with nanofabrication, and D. Ziegler for samples of parylene-C.

Supporting Information Available

SEM images of nanotube fabrication using PMMA protective polymer. This material is available free of charge *via* the Internet at http://pubs.acs.org

References

[1] Campbell, N. A.; Reece, J. B.; Taylor, M. R.; Simon, E. J. *Biology: Concepts & Connections*, 5th ed.; Educational Pearson: New York, 2006.

[2] Blankenship, R. E.; Tiede, D. M.; Barber, J.; Brudvig, G. W.; Fleming, G. R.; Ghirardi, M.; Gunner, M. R.; Junge, W.; Kramer, D. M.; Melius, A. *et al.* Comparing Photosynthetic Efficiencies and Recognizing the Potential for Improvement. *Science* **2011**, *332*, 805-809.

[3] Reece, S. Y.; Hamel, J. A.; Sung, K.; Jarvi, T. D.; Esswein, A. J.; Pijpers, J. J. H.; Nocera, D. G. Wireless Solar Water Splitting Using Silicon-Based Semiconductors and Earth-Abundant Catalysts. *Science* **2011**, *334*, 645-648.

[4] Verlage, E.; Hu, S.; Liu, R.; Jones, J. R.; Sun, K.; Xiang, C.; Lewis, N. S.; Atwater, H. A. A Monolithically Integrated, Intrinsically Safe, 10% Efficient, Solar-Driven Water-Splitting System Based on Active, Stable Earth-Abundant Electrocatalysts in Conjunction with Tandem III-V Light Absorbers Protected by Amorphous TiO_2 Films. *Energy Environ. Sci.* **2015**, *8*, 3166-3172.

[5] Sun, K.; Liu, R.; Chen, Y.; Verlage, E.; Lewis, N. S.; Xiang, C. A Stabilized, Intrinsically Safe, 10% Efficient, Solar-driven Water-splitting Cell Incorporating Earth-Abundant Electrocatalysts with Steady-State pH Gradients and Product Separation Enabled by a Bipolar Membrane. *Adv. Energy Mater.* **2016**, *6*, 1600379.

[6] Khaselev, O.; Turner, J. A. A Monolithic Photovoltaic-Photoelectrochemical Device for Hydrogen Production via Water Splitting. *Science* **1998**, *280*, 425-427.

[7] Young, J. L.; Steiner, M. A.; Doescher, H.; France, R. M.; Turner, J. A.; Deutsch, T. G. Direct Solar-to-Hydrogen Conversion via Inverted Metamorphic Multi-Junction Semiconductor Architectures. *Nature Energy* **2017**, *2*, 17028.

[8] Brillet, J.; Yum, J. H.; Cornuz, M.; Hisatomi, T.; Solarska, R.; Augustynski, J.; Gratzel, M.; Sivula, K. Highly Efficient Water Splitting by a Dual-Absorber Tandem Cell. *Nature Photonics* **2012**, *6*, 824-828.

[9] Abdi, F. F.; Han, L.; Smets, A. H. M.; Zeman, M.; Dam, B.; van de Krol, R. Efficient Solar Water Splitting by Enhanced Charge Separation in a Bismuth Vanadate-Silicon Tandem Photoelectrode. *Nature Commun.* **2013**, *4*, 2195.

[10] Jang, J. W.; Du, C.; Ye, Y.; Lin, Y.; Yao, X.; Thorne, J.; Liu, E.; McMahon, G.; Zhu, J.; Javey, A.; Guo, J.; Wang, D. Enabling Unassisted Solar Water Splitting by Iron Oxide and Silicon. *Nature Commun.* **2015**, *6*, 7447.

[11] Liu, C.; Tang, J.; Chen, H.M.; Liu, B.; Yang, P. A Fully Integrated Nanosystem of Semiconductor Nanowires for Direct Solar Water Splitting. *Nano Lett.* **2013**, *13*, 2989.

[12] Liu, B.; Wu, C. H.; Miao, J.; Yang, P. All-Inorganic Semiconductor Nanowire Mesh for Direct Solar Water Splitting. *ACS Nano* **2014**, *8*, 11739-11744.

[13] Shaner, M. R.; Fountaine, K. T.; Ardo, S.; Coridan, R. H.; Atwater, H. A.; Lewis, N. S. Photoelectrochemistry of Core-Shell Tandem Junction n-p^+-Si/n-WO_3 Microwire Array Photoelectrodes. *Energy Environ. Sci.* **2014**, *7*, 779-790.

[14] Nocera, D. G. The Artificial Leaf. *Acc. Chem. Res.* **2012**, *45*, 767-776.

[15] Luo, J; Im, J. M.; Mayer, M. T.; Schreier, M.; Nazeeruddin, M. K.; Park, N. G.; Tilley, S. D.; Fan. H. J.; Graetzel, M. Water Photolysis at 12.3% Efficiency via Perovskite Photovoltaics and Earth-Abundant Catalysts. *Science* **2014**, *345*, 1593-1596.

[16] Chabi, S.; Papadantonakis, K. M.; Lewis, N. S.; Freund, M. S. Membranes for Artificial Photosynthesis. *Energy Environ. Sci.* **2017**, 10, 1320-1338.

[17] Arai, T.; Sato. S.; Morikawa, T. A Monolithic Device for CO_2 Photoreduction to Generate Liquid Organic Substances in a Single-Compartment Reactor. *Energy Environ. Sci.* **2015**, *8*, 1998-2002.

[18] Schreier, M.; Curvat, L.; Giordano, F.; Steier, L.; Abate, A.; Zakeeruddin, S. M.; Luo, J.; Mayer, M. T.; Graetzel, M. Efficient Photosynthesis of Carbon Monoxide from CO_2 using Perovskite Photovoltaics. *Nature Commun.* **2015**, *6*, 7326.

[19] Zhou, X.; Liu, R.; Sun, K.; Chen, Y.; Verlage, E.; Francis, S. A.; Lewis, N. S.; Xiang, C. Solar-driven Reduction of 1 atm of CO_2 to Formate at 10% Energy-Conversion Efficiency by Use of a TiO_2-Protected III-V Tandem Photoanode in Conjunction with a Bipolar Membrane and a Pd/C Cathode. *ACS Energy Lett.* **2016**, *1*, 764-770.

[20] Kim, W.; McClure, B. A.; Edri, E.; Frei, H. Coupling Carbon Dioxide Reduction with Water Oxidation in Nanoscale Photocatalytic Assemblies. *Chem. Soc. Rev.* **2016**, *45*, 3221-3243.

[21] Kim, W.; Edri, E.; Frei, H. Hierarchical Inorganic Assemblies for Artificial Photosynthesis. *Acc. Chem. Res.* **2016**, *49*, 1634-1645.

[22] Kim, W.; Yuan, G.; McClure, B. A.; Frei, H. Light Induced Carbon Dioxide Reduction by Water at Binuclear $ZrOCo^{II}$ Unit Coupled to Ir Oxide Nanocluster Catalyst. *J. Am. Chem. Soc.* **2014**, *136*, 11034-11042.

[23] Yuan, G.; Agiral, A.; Pellet, N.; Kim, W.; Frei, H. Inorganic Core-Shell Assemblies for Closing the Artificial Photosynthetic Cycle. *Faraday Discuss.* **2014**, *176*, 233-249.

[24] Agiral, A.; Soo, H. S.; Frei, H. Visible Light Induced Hole Transport from Sensitizer to Co_3O_4 Water Oxidation Catalyst across Nanoscale Silica Barrier with Embedded Molecular Wires. *Chem. Mater.* **2013**, *25*, 2264-2273.

[25] Edri, E.; Frei, H. Charge Transport Through Organic Molecular Wires Embedded in Ultrathin Insulating Inorganic Layer. *J. Phys. Chem. C* **2015**, *119*, 28326-28334.

[26] Soo, H. S.; Agiral, A.; Bachmeier, A.; Frei, H. Visible Light-Induced Hole Injection into Rectifying Molecular Wires Anchored on Co_3O_4 and SiO_2 Nanoparticles. *J. Am. Chem. Soc.* **2012**, *134*, 17104-17116.

[27] Edri, E.; Cooper, J. K.; Sharp, I. D.; Guldi, D. M.; Frei, H. Ultrafast Charge Transfer between Light Absorber and Co_3O_4 Water Oxidation Catalyst across Molecular Wires Embedded in Silica Membrane. *J. Am. Chem. Soc.* **2017**, *139*, 5458-5466.

[28] Elias, J.; Tena-Zaera, R.; Wang, G. Y.; Levy-Clement, C. Conversion of ZnO Nanowires into Nanotubes with Tailored Dimensions. *Chem. Mater.* **2008**, *20*, 6633-6637.

[29] Roy, P.; Berger, S.; Schmuki, P. TiO_2 nanotubes: Synthesis and Applications. *Angew. Chem. Int. Ed.* **2011**, *50*, 2904-2939.

[30] Martinson, A. B. F.; Elam, J. W.; Hupp, J. T.; Pellin, M. J. ZnO Nanotube Based Dye-Sensitized Solar Cells. *Nano Lett.* **2007**, *7*, 2183-2187.

[31] Dloczik, L.; Engelhardt, R.; Ernst, K.; Fiechter, S.; Sieber, I.; Koenenkamp, R. Hexagonal Nanotubes of ZnS by Chemical Conversion of Monocrystalline ZnO Columns. *Appl. Phys. Lett.* **2001**, *78*, 3687-3689.

[32] Hwang, J.; Min, B.; Lee, J. S.; Keem, K.; Cho, K.; Sung, M. Y.; Lee, M. S.; Kim, S. Al_2O_3 Nanotubes Fabricated by Wet Etching of ZnO/Al_2O_3 Core/Shell Nanofibers. *Adv. Mater.* **2004**, *16*, 422-425.

[33] Guan, C.; Xia, X.; Meng, N.; Zeng, Z.; Cao, X.; Soci, C.; Zhang, H.; Fan, H. J. Hollow Core-Shell Nanostructure Supercapacitor Electrodes: Gap Matters. *Energy Environ. Sci.* **2012**, *5*, 9085-9090.

[34] Joshi, R. K.; Schneider, J. J. Assembly of One-Dimensional Inorganic Nanostructures into Functional 2D and 3D Architectures. Synthesis, Arrangement and Functionality. *Chem. Soc. Rev.* **2012**, *41*, 5285-5312.

[35] Lakshmi, B. B.; Patrissi, C. J.; Martin, C. R. Sol-Gel Template Synthesis of Semiconductor Oxide Micro- and Nanostructures. *Chem. Mater.* **1997**, *9*, 2544-2550.

[36] Park, H. A.; Liu, S.; Oh, Y.; Salvador, P. A.; Rohrer, G. S.; Islam, M. F. Nano-Photoelectrochemical Cell Arrays with Spatially Isolated Oxidation and Reduction Channels. *ACS Nano* **2017**, *11*, 2150-2159.

[37] Li, L.; Zhai, T.; Zeng, H.; Fang, X.; Bando, Y.; Golberg, D. Polystyrene Sphere-Assisted One-Dimensional Nanostructure Arrays: Synthesis and Applications. *J. Mater. Chem.* **2011**, *21*, 40-56.

[38] Welch, C. C.; Olynick, D. L.; Liu, Z.; Holmberg, A.; Peroz, C.; Robinson, A. P. G.; Henry, M. D.; Scherer, A.; Mollenhauer, T.; Genova, V.; Ng, D. K. T. Formation of Nanoscale Structures by Inductively Coupled Plasma Etching. *Proc. SPIE* **2012**, *8700*, 870002-1-19.

[39] Liu, Z.; Wu, Y.; Harteneck, B.; Olynick, D. Super-Selective Cryogenic Etching for Sub-10 nm Features. *Nanotechnology* **2013**, *24*, 15305-15312.

[40] Elam, J. W.; Routkevitch, D.; Mardilovich, P. P.; George, S. M. Conformal Coating on Ultrahigh-Aspect-Ratio Nanopores of Anodic Alumina by Atomic Layer Deposition. *Chem. Mater.* **2003**, *15*, 3507-3517.

[41] Parsons, G. N.; George, S. M.; Knez;, M. Progress and Future Directions for Atomic Layer Deposition and ALD Based Chemistry. *MRS Bulletin* **2011**, *36*, 865-871.

[42] Hämäläinen, J.; Ritala, M.; Leskelä, M. Atomic Layer Deposition of Noble Metals and Their oxides. *Chem. Mater.* **2014**, *26*, 786–801.

[43] Colthup, N. B.; Daly, L. H.; Wiberley, S. E. *Introduction to Infrared and Raman Spectroscopy*, 3rd ed.; Academic Press: New York, 1990.

[44] Han, H.; Frei, H. *In situ* Spectroscopy of Water Oxidation at Ir oxide Nanocluster Driven by Visible TiOCr Charge-Transfer Chromophore in Mesoporous Silica. *J. Phys. Chem. C* **2008**, *112*, 16156-16159.

[45] Kim, W.; Frei, H. Directed Assembly of Cuprous Oxide Nanocatalyst for CO_2 Reduction Coupled to Heterobinuclear $ZrOCo^{II}$ Light Absorber in Mesoporous Silica. *ACS Catal.* **2015**, *5*, 5627-5635.

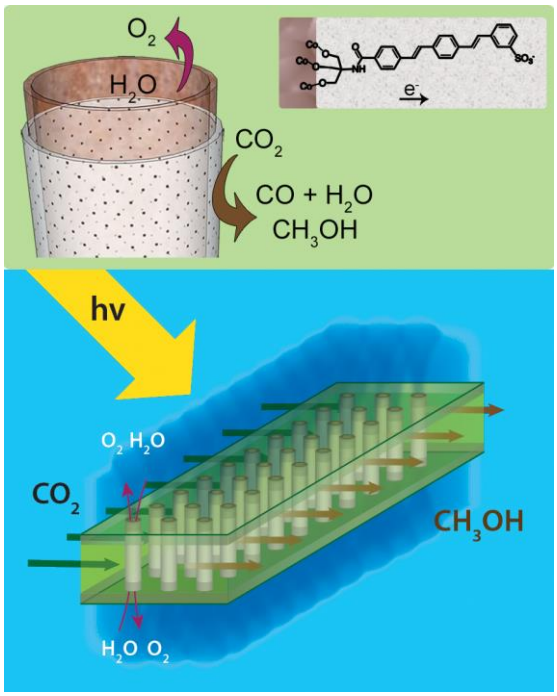

Figure 1: Functionalized Co oxide – silica core-shell nanotubes as complete artificial photosynthetic units in the form of a macroscale array for CO_2 reduction by H_2O under membrane separation. Top: Sketch of individual core-shell nanotube showing silica-embedded *oligo*-para(phenylene vinylene) molecular wires (inset). Bottom: Array of nanotubes with separation of oxygen evolution space inside the tubes from CO_2 reduction space between the tubes.

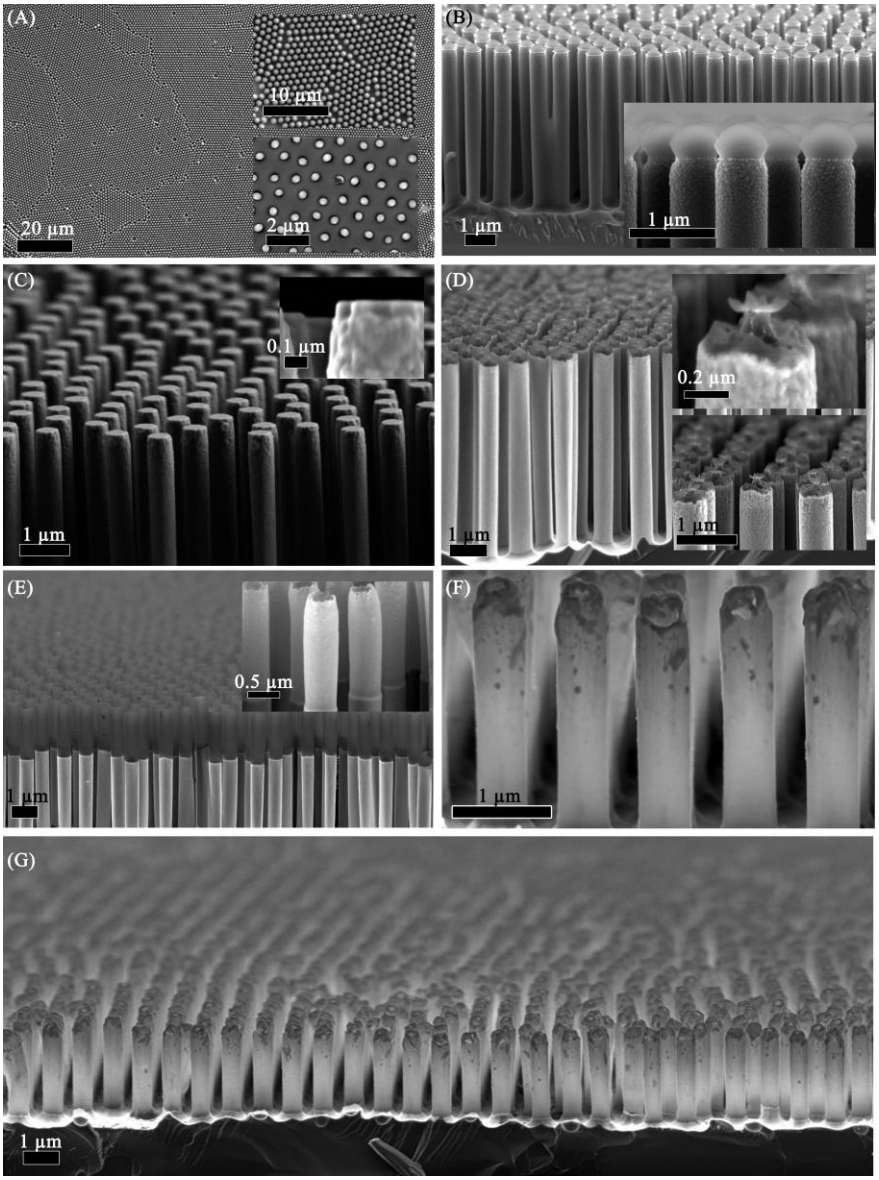

Figure 2: SEM images of fabrication steps of core-shell nanotube array. (A) A layer of polystyrene beads on Si wafer showing a 100-200 µm large 2D crystalline structure. Top inset: Higher magnification of polystyrene beads layer showing close packing of the crystalline beads. Lower inset: Polystyrene beads layer after O_2 plasma etching of ~50% of the bead diameter. (B) Slightly angled side view image of the Si rods after cryo-etching with the beads on top. Inset: higher magnification side view showing a slightly roughened surface near the upper part of the rods in comparison to the smooth surface of the rods. (C) Si rod array after bead removal and deposition of Co_3O_4 and SiO_2 layers. Inset: higher magnification of side view top of a rod. (D) Slightly angled side view image of SiO_2 on Si/Co_3O_4 array with Al_2O_3 coating followed by opening of top end. Insets: higher magnification images of opened top end. The formation of a tube is apparent along the rim of the rod. (E) An array of partly-etched core-shell tubes. Approximately 1.5 µm of the Si core was removed. (F) An array of fully etched core-shell nanotube array with Si support. (G) A low magnification image of a fully etched core-shell nanotube array with Si support.

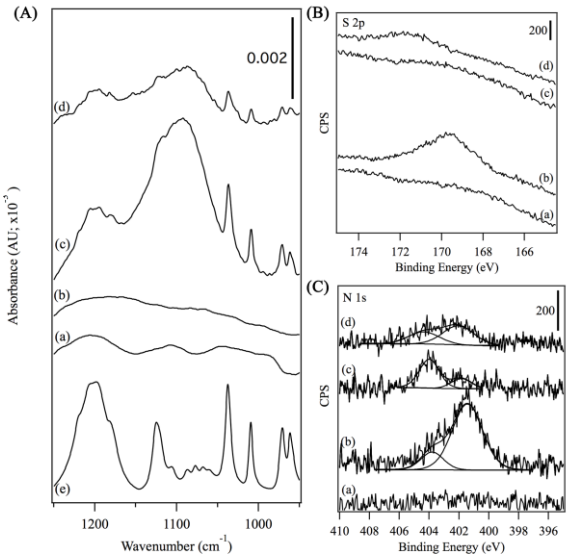

Figure 3: FT-IR and XPS spectra of Si nanorod array with core-shell deposits indicating the presence and integrity of PV3_tripod molecules in the ultrathin SiO_2 nanotube shell. (A) (a) GAATR FT-IR spectra of Si rod/Co_3O_4. (b) Pure SiO_2 on Si rod/Co_3O_4. (c) PV3_tripod on Si rod/Co_3O_4. (d) SiO_2-encapsulated PV3_tripod on Si rod/Co_3O_4. (e) Absorbance FT-IR spectrum of pure PV3_tripod sample in KBr. All GAATR FT-IR spectra were recorded at 62.5° incident angle and 4 cm^{-1} resolution. Baseline is ATR crystal versus air. (B) S 2p XPS spectra of (a) Si rod/Co_3O_4. (b) PV3_tripod on Si rod/Co_3O_4. (c) Pure SiO_2 on Si rod/Co_3O_4. (d) SiO_2-encapsulated PV3_tripod on Si rod/Co_3O_4. (C) N 1s XPS spectra of (a) Si rod/Co_3O_4. (b) PV3_tripod on Si rod/Co_3O_4. (c) Pure SiO_2 on Si rod/Co_3O_4. (d) SiO_2-encapsulated PV3_tripod on Si rod/Co_3O_4. Data not corrected for charging. XPS spectral analysis was done with software CasaXPS V2.3.

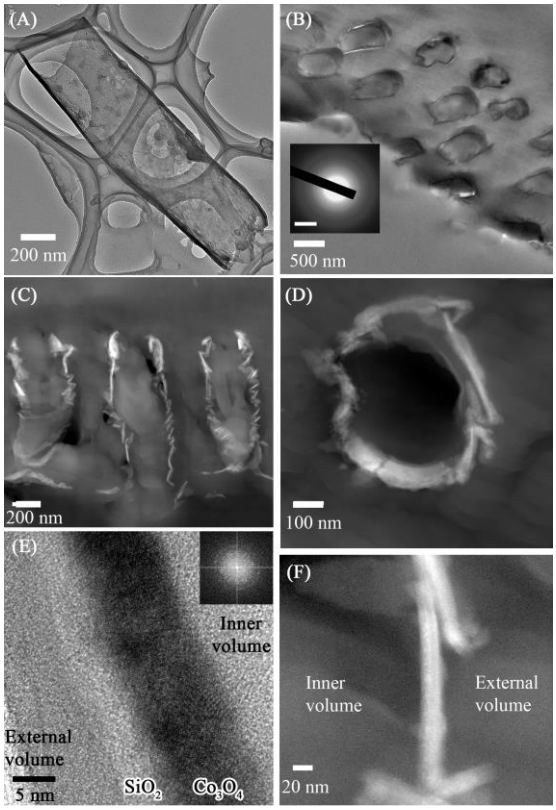

Figure 4: Transmission electron microscopic images of core-shell tube. (A) Tube supported by holey carbon support and (B) HAADF-STEM image of transverse cross-section of a tube array embedded in parylene-C. (C) Longitudinal cross-section HAADF-STEM image of three tubes showing the open top and empty interior of the tubes with some of the tube support at the bottom still apparent. The inset shows the electron diffraction pattern indicating the polycrystalline nature of the Co_3O_4 layer. (D) Medium magnification HAADF-STEM image of a single tube transverse cross-section. (E) High resolution TEM image of a longitudinal cross-section image of a tube showing the crystalline 12 nm thick Co_3O_4 layer on the inner volume side of the tube, coated with a 2 nm thick SiO_2 layer and protected with a 10 nm thick Al_2O_3 layer on the external side of the tube. Inset is FFT of the Co_3O_4 layer showing crystallinity. (F) High magnification HAADF-STEM image of part of transverse cross-section of a tube showing the core-shell structure of the tube.

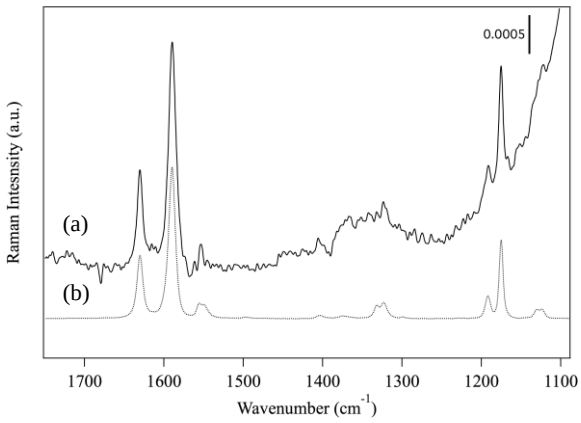

Figure 5: (a) FT-Raman spectra of empty SiO_2-encapsulated PV3_tripod on Co_3O_4 core-shell nanotubes after edging of sacrificial Si rods. Resolution 2 cm^{-1}, 152 mW Nd:Yag laser power, 25600 scans. (b) Spectrum of pure PV3_tripod powder.

TOC Graphics